ADVANCED ENERGY MATERIALS
www.advenergymat.de

Carbon-Tailored Semimetal MoP as an Efficient Hydrogen Evolution Electrocatalyst in Both Alkaline and Acid Media

Guowei Li, Yan Sun, Jiancun Rao, Jiquan Wu, Anil Kumar, Qiu Nan Xu, Chenguang Fu, Enke Liu, Graeme R. Blake, Peter Werner, Baiqi Shao, Kai Liu, Stuart Parkin, Xianjie Liu, Mats Fahlman, Sz-Chian Liou, Gudrun Auffermann, Jian Zhang, Claudia Felser,* and Xinliang Feng**

The electrolysis processes such as hydrogen evolution reaction (HER) require high efficient catalysts with robust surface stability. A high conductivity is also necessary to speed up the charge transport between the catalyst and the electrolyte. Recently, the observation of exceedingly high conductivity in the topological semimetal MoP, has provided a model catalyst to investigate the correlation between the electrical transport and the electrocatalytic activity for the HER. Thus, MoP is encapsulated in a Mo, P codoped carbon layer (MoP@C). This composite material exhibits outstanding HER performance, with an extremely low overpotential of 49 mV at a current density of 10 mA cm^{-2} and a Tafel slope of 54 mV dec^{-1} in an alkaline medium. In addition, electron transport analysis indicates that MoP exhibits high conductivity and mobility due to the existence of triple-point fermions and a complex Fermi surface. Furthermore, the presence of P—C and Mo—C bonds at the interface between the carbon layer and the MoP particles modulates the band structure of MoP@C and facilitates fast electron transfer, accumulation, and subsequent delocalization, which are in turn responsible for the excellent HER activity.

In recent decades, the ongoing energy crisis and issues related to environmental pollution have motivated the research community to search for alternative and renewable forms of energy.[1] In this context, hydrogen is a promising alternative to conventional energy sources due to its clean nature (i.e., only water is produced upon burning) and high energy density.[2] The electrochemical splitting of water to yield high purity hydrogen (>99.6%) has therefore drawn increasing attention.[3] However, due to the sluggish kinetics of the HER, the use of electrocatalysts is essential in order to reduce the overpotential, especially in alkaline solutions. Although Pt and Pt-based alloys are still benchmark electrocatalysts in the HER, the high cost and low abundance of Pt limits its widespread application in hydrogen production technologies.

Recently, a range of abundant transition metal phosphides such as molybdenum phosphide have been intensively examined as potential HER electrocatalysts. Various strategies have been employed to improve the electrocatalytic HER activity of transition metal phosphides, including surface phosphosulfidation, hybridization, and elemental doping.[4] However, despite such modifications, MoP continues to suffer from a high overpotential (>130 mV at 10 mA cm^{-2})[5] and significant

Dr. G. Li, Dr. Y. Sun, Dr. Q. N. Xu, Dr. C. Fu, Dr. E. Liu, Dr. G. Auffermann, Prof. C. Felser
Max Planck Institute for Chemical Physics of Solids
01187 Dresden, Germany
E-mail: Claudia.Felser@cpfs.mpg.de
Dr. J. Rao, Dr. S.-C. Liou
AIM Lab
Maryland NanoCenter
University of Maryland
MD 20742, USA
The ORCID identification number(s) for the author(s) of this article can be found under https://doi.org/10.1002/aenm.201801258.

DOI: 10.1002/aenm.201801258

Dr. J. Wu, Dr. X. Liu, Prof. M. Fahlman
Department of Physics
Chemistry and Biology (IFM)
Linköping University
58183 Linköping, Sweden
Dr. A. Kumar, Dr. G. R. Blake
Zernike Institute for Advanced Materials
University of Groningen
9747 AG Groningen, The Netherlands
Dr. P. Werner, Prof. S. Parkin
Max Planck Institute for Microstructure Physics
D - 06120 Halle, Germany
Dr. B. Shao, Prof. K. Liu
State Key Laboratory of Rare Earth Resource Utilization
Changchun Institute of Applied Chemistry
Chinese Academy of Sciences
130022 Changchun, China
Dr. J. Zhang, Prof. X. Feng
Center for Advancing Electronics Dresden (cfaed) & Department of Chemistry and Food Chemistry
Technische Universität Dresden
01062 Dresden, Germany
E-mail: jian.zhang1@tu-dresden.de; xinliang.feng@tu-dresden.de

instability in alkaline electrolytes. Here we investigate whether the topological states of MoP can be exploited to improve its electrocatalytic performance. Topologically nontrivial semimetals have recently been reported for a variety of thin films and 3D materials, and such reports have greatly inspired frontline research in which their exotic physical properties and possible applications are explored. For example, topological semimetals exhibit protected and robust surface states while their time reversal symmetry is preserved as a result of the topological invariant.[6] The linear dispersion of the band structure in the bulk state and the topologically protected surface Fermi arcs result in unique properties, such as extremely large magnetoresistance and ultrahigh mobility.[7] Very recently, pairs of Weyl points, three-component fermions, and superconductivity have been theoretically and experimentally verified in the bulk electronic structure of MoP crystals.[8] Indeed, our group has revealed a low resistivity for MoP (6 nΩ at 2 K and 8.2 μΩ at 300 K) in addition to a promising charge carrier density (≈1.1×10^{23} cm^{-3} at 300 K).[9] Thus, we first calculated the Z_2 invariants by the evolution of Wannier centers during a "time-reversal pumping" process. Although MoP is a semimetal without a global gap, its bands in the $k_3 = 0$ and $k_3 = \pi$ planes are fully gapped, leading to a defined Z_2 topological charge in these two planes. As shown in Figure S1a–c of the Supporting Information, the Z_2 was calculated to be 1 and 0 for the $k_z = 0$ and $k_z = \pi$ planes, respectively. Therefore, MoP hosts nonzero topological charge, which leads to a topologically protected surface state. It should be noted here that the topological state is a result of the topologically nontrivial nature of its band structure, which is generated by the spin–orbit interaction or nonsymmorphic symmetry. These are robust and protected by time-reversal symmetry, and do not depend on size or possible surface defects and doping. In order to simulate nanostructured MoP, we established a slab structure with 60 unit cell layers using a tight-binding Hamiltonian.[10] As illustrated in **Figure 1**a, the bulk and surface states can be seen clearly. The Weyl point is observed in the k-path of the GK direction, in accordance with ARPES measurements of the bulk MoP structure.[8a] Such surface properties are advantageous in the context of the electrochemical reactions taking place on electrocatalyst surfaces, thereby indicating the possibility of tailoring MoP into an excellent HER electrocatalyst.

With this aim in mind, we herein report the preparation of a MoP@C electrocatalyst, where polycrystalline MoP nanoparticles are embedded in a Mo- and P-codoped amorphous carbon layer. We find that the electrical transport near room temperature is dominated by the Mott variable-range hopping mechanism in the MoP@C electrocatalyst, confirming that carbon coating results in electron localization. In addition, the presence of Mo—C and P—C bonds between MoP and the amorphous carbon layer reshape the Fermi energy of the MoP electrocatalyst

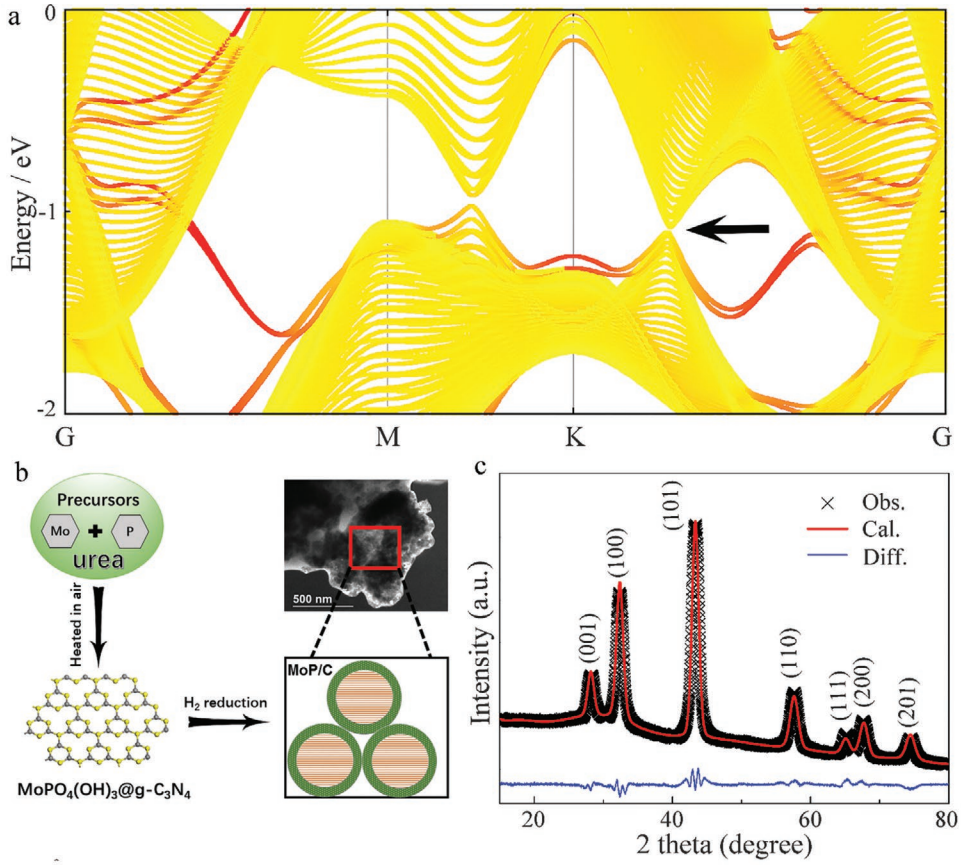

Figure 1. a) Band structure of MoP based on slab structure with 60 unit cell layers (red: surface state bands; yellow: bulk state bands). b) Schematic illustration of the synthetic route employed for preparation of the Mo- and P-codoped MoP@C catalyst. c) Observed (black data points), calculated (red line), and difference (blue line) XRD patterns of the as-prepared sample.

and delocalize the accumulated electrons, thereby accelerating the HER kinetics on the MoP@C electrocatalyst surface with an extremely decreased overpotential of 49 mV at a current density of 10 mA cm^{-2} and a small Tafel slope of 54 mV dec^{-1}. These values are superior or comparable to previously reported non-noble-metal-based HER electrocatalysts and Pt catalysts.

The process employed for preparation of the MoP@C electrocatalyst is illustrated in Figure 1b. A pretreated carbon cloth (CC) was immersed in a solution containing $(NH_4)_6Mo_7O_{24}$ (0.5 mmol), citric acid (4 mmol), urea (33 mmol), and $(NH_4)_2HPO_4$ (4 mmol). Drying at 80 °C produced a Mo complex on the CC, and subsequent heating at 500 °C for 4 h under air gave the Mo—P precursor/g-C_3N_4. Finally, treatment at 850 °C under H_2 for 2 h gave the desired MoP@C electrocatalyst (full experimental details are given in the Supporting Information). The obtained electrocatalyst was then examined by X-ray powder diffraction (XRD), with the resulting pattern corresponding to the hexagonal structure of MoP (Figure 1c; Table S1, Supporting Information, JCPDS no. 89–5110, $a = b = 3.22$ Å and $c = 3.20$ Å), with peaks indexed to the (001), (100), (101), (110), (111), (200), and ($\bar{2}$01) planes being observed. This result is consistent with the $P\bar{6}2m$ space group, in which Mo and P occupy 1a and 1d Wyckoff positions with position coordinates of (0,0,0) and (1/3,2/3,1/2), respectively.

The morphology of the electrocatalyst was then investigated by transmission electron microscopy (TEM) and high-angle annular dark-field imaging scanning transmission electron microscopy (HAADF-STEM). As shown in **Figure 2**a and Figure S2a (Supporting Information), irregular nanocrystals with diameters of tens of nanometers were randomly embedded

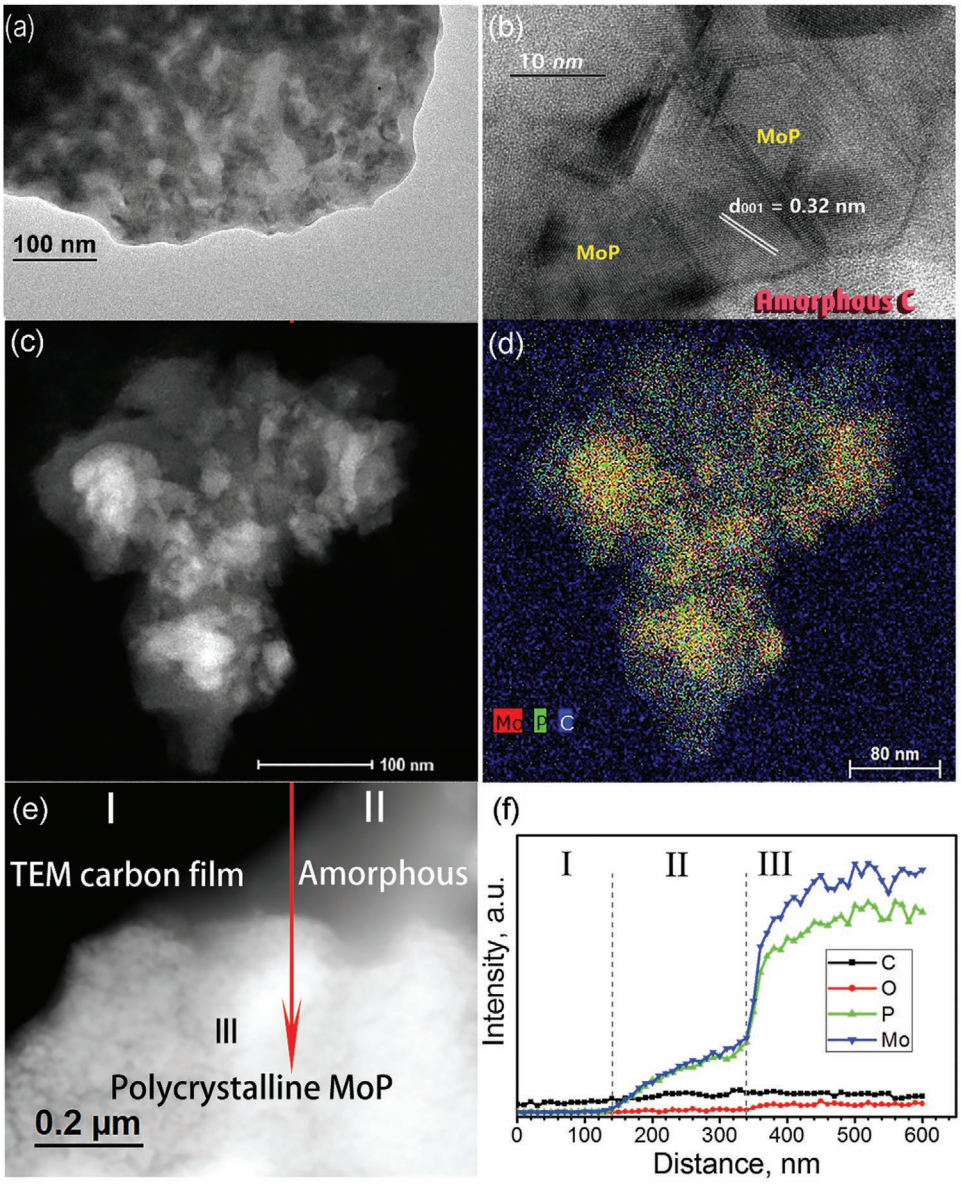

Figure 2. a) TEM and b) HRTEM images of the MoP@C catalyst. c) HAADF and d) corresponding elemental mapping images. e) HAADF image with the EDS line-scanning direction indicated by a red arrow. f) Position-dependent EDS line-scan results.

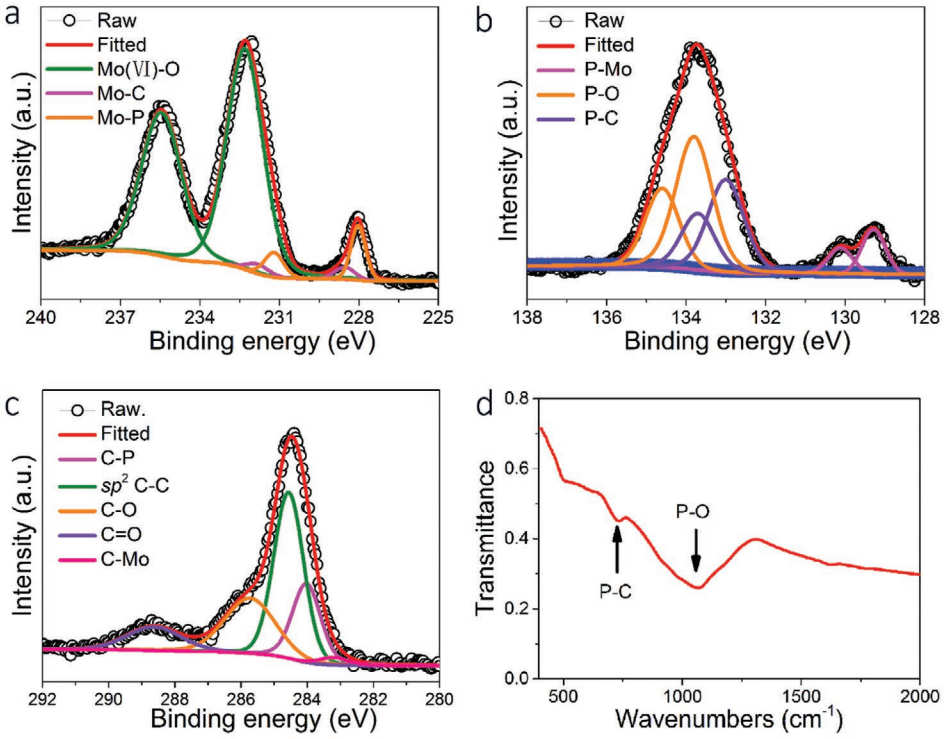

Figure 3. High-resolution XPS on the MoP@C catalyst: a) Mo 3d, b) P 2p, and c) C 1s spectra. d) IR spectrum of MoP@C catalyst.

in the amorphous carbon layer. In the HRTEM image in Figure 2b, the *d*-spacing of 0.32 nm could be attributed to the (001) plane of the MoP hexagonal phase. Selected-area electron diffraction analysis of the prepared MoP@C revealed a series of rings, indicating the polycrystalline nature of this material, the *d*-spacings of which are consistent with the hexagonal MoP phase (Figure S2b, Supporting Information). Furthermore, elemental mapping by energy dispersive spectroscopy (EDS) confirmed the presence of Mo, P, and C in the electrocatalyst (Figure 2c,d; Figure S3a–d, Supporting Information). The ratio of Mo to P is close to the nominal value of 1 for both bare MoP and MoP@C samples (Figure S4, Supporting Information). As expected, carbon was found over the full area examined, with traces of Mo and P also being detected in the carbon layers. EDS elemental line-scanning was then carried out, as shown in the HAADF image (see Figure 2e,f). Both Mo and P were detected immediately when the electron probe was positioned on the amorphous carbon layer. These results unambiguously confirm that the amorphous carbon contains C, P, Mo, and O. The thermal stability of the MoP@C electrocatalyst was then examined under argon using thermogravimetric analysis (Figure S5, Supporting Information). The onset of rapid weight loss indicated that bare MoP decomposed rapidly at ≈900 °C, while MoP@C was remarkably stable, with no decomposition being observed below 1300 °C.

The surface chemical bonding characteristics of the MoP@C electrocatalyst were analyzed by X-ray photoelectron spectroscopy (XPS), where the survey spectrum confirmed that it consisted of Mo, P, C, and O (Figure S6, Supporting Information). In addition, in the high-resolution Mo 3d and P 2p spectra, the peaks observed at 232.4 and 133.8 eV correspond to the Mo $3d_{3/2}$ and P 2p binding energies, respectively, which originate from surface oxidation of the metastable MoP.[4d,11] Doublets at binding energies of 228.0 (Mo $3d_{3/2}$) and 129.3 eV (P 2p) are attributed to the molybdenum and phosphorus present in MoP.[4b,12] Moreover, in a three component fit of the Mo and P spectra, contributions from covalent Mo—C (228.5 eV) and P—C (133.0 eV) bonds are apparent, suggesting the presence of strong chemical interactions between the carbon layer and the MoP nanoparticles (**Figure 3**c).[13] In the core-level C1s spectra, peaks assigned to C—P (283.2 eV) and C—Mo (284.0 eV) bonds are also observed, in addition to the main peak of amorphous carbon centered at 284.6 eV.[13c,14] Subsequent XPS depth profiling confirmed that the C—P and Mo—C bonds are localized in the carbon layer and at the interfaces between carbon and the MoP nanoparticles. The interaction between phosphorus and carbon was further demonstrated by Fourier transform infrared spectroscopy (FT-IR) (Figure 3d). Apart from the P—O stretching mode at 1064 cm^{-1}, the stretching of P—C bonds was also observed at 726 cm^{-1}, consistent with reported characteristic frequencies in the range of 650–758 cm^{-1}.[14,15] Such bonds can be considered important in the context of stabilizing the interface and enhancing the electrochemical stability of the resulting electrocatalyst.

The electrocatalytic HER activities of the MoP and MoP@C electrocatalysts were then determined using a standard three-electrode setup in an aqueous 1 M KOH and 0.5 M H_2SO_4 solution. All potentials quoted herein are referenced versus the reversible hydrogen potential. The corresponding polarization curves with *iR* compensation are shown in **Figure 4**a. The Pt/C catalyst only required an overpotential (η) of 29 mV to deliver a current density of 10 mA cm^{-2}. By contrast, bare MoP afforded a current density of 10 mA cm^{-2} at 154 mV.

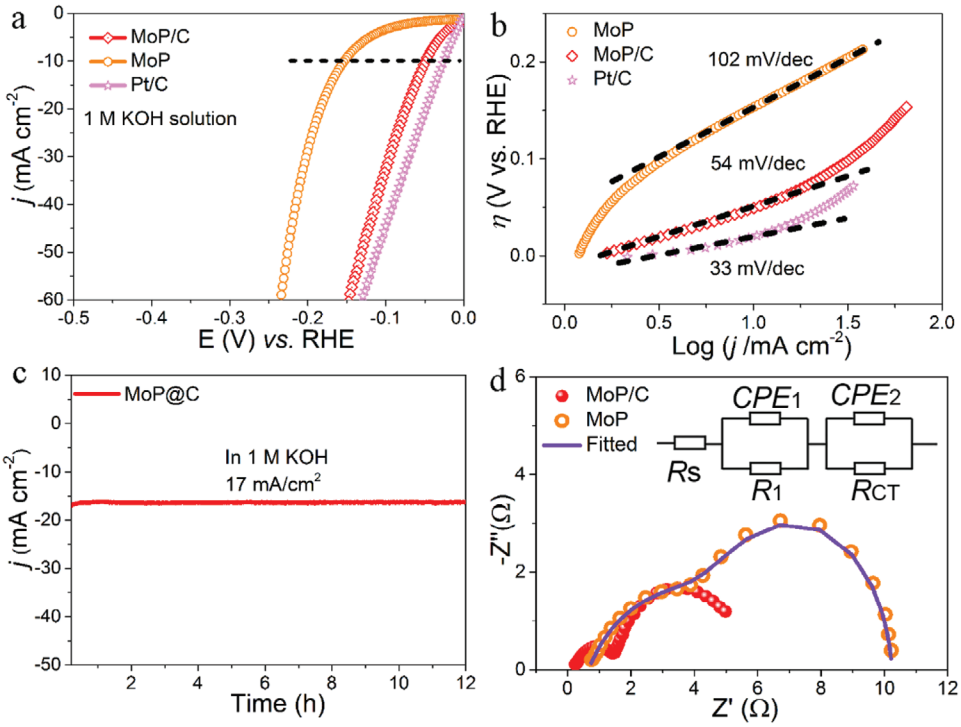

Figure 4. a) HER polarization curves and b) Tafel plots of the MoP, MoP@C, and 20% Pt/C catalysts in a 1 M KOH solution. c) Chronoamperometric responses recorded for MoP@C using a current density of 17 mA cm^{-2} at a constant overpotential of 72 mV with *iR* compensation. d) EIS Nyquist plots, fitted with the two-time constant model.

Remarkably, the HER on MoP@C occurred at 0 mV and the overpotential of this sample decreased significantly to 49 mV, which represents superior HER activity compared to other MoP electrocatalysts, and exceeds the activities of the majority of non-noble-metal HER electrocatalysts such as MoP nanoparticles (i.e., 130 mV at 10 mA cm^{-2}),[5] MoP/graphene oxide composites (162 mV at 10 mA cm^{-2}),[12a] Mo_2C nanooctahedra (151 mV at 10 mA cm^{-2}),[16] CoP nanoparticles on CC (115 mV at 10 mA cm^{-2}),[17] and FeP nanorod arrays (218 mV at 10 mA cm^{-2})[18] (Table S2, Supporting Information). Additionally, the cathodic current density of the prepared MoP@C was significantly larger than that of Pt/C at an overpotential of 220 mV (Figure S7, Supporting Information). Tafel plots were then employed to further investigate the HER kinetics of the electrocatalysts (Figure 4b and **Table 1**). Here, Pt/C exhibited the lowest Tafel slope of 33 mV dec^{-1}, suggesting that the Tafel reaction was the rate-limiting step. By comparison, the Tafel slope of the bare MoP sample was 102 mV dec^{-1}. However, the Tafel slope of the prepared MoP@C was 54 mV dec^{-1}, indicating that the HER kinetics of this material follow the Volmer–Heyrovsky mechanism.[19] Interestingly, the exchange current density of the MoP@C sample was determined to be 0.69 mA cm^{-2}, which outperforms the bare MoP sample (0.29 mA cm^{-2}), Pt/C (0.52 mA cm^{-2}), and other well-known Mo-based electrocatalysts (Table S2, Supporting Information). The stability of the MoP@C catalyst was subsequently evaluated by long-term electrolysis at a constant overpotential (Figure 4c). The current density remained stable over 12 h, and no significant changes to the crystal structure were observed by XRD measurements following the stability test (Figure S8, Supporting Information). The Faradaic efficiency of the MoP@C catalyst was determined to be about 100% by comparing the theoretical and experimentally produced H_2 quantities (Figure S9, Supporting Information). The electrocatalytic HER activity of the MoP and MoP@C catalysts in 0.5 M H_2SO_4 was also investigated. The overpotential at a current density of 10 mA cm^{-2} substantially decreased from 150 mV for MoP to 88 mV for MoP@C. The Tafel slopes of the MoP and MoP@C samples were 76 and 50.4 mV dec^{-1}, respectively (Figure S10a,b, Supporting Information). After 2000 CV cycles, the overpotential at 10 mA cm^{-2} showed negligible change (Figure S10c, Supporting Information), reflecting superior durability in acidic solution.

Table 1. Comparison of the catalytic parameters of different HER catalysts in a 1 M KOH electrolyte.

Catalyst	η [10 mA cm^{-2}]	Tafel slope	j_0 [mA cm^{-2}]
MoP	154	102	0.29
MoP@C	49	54	0.69
Pt/C	27	33	0.52

Electrochemical impedance spectroscopy (EIS) was then performed in an effort to understand the electrode kinetics of the HER process (Figure 4d). As shown in the figure, the Nyquist plots of both MoP and MoP@C consisted of two semicircles in the high-medium frequency and low frequency regions. Circuit model fitting analysis showed that both Nyquist plots can be modeled using a two-time-constant model consisting of a solution resistance (R_S), in series with two parallel resistor combinations (R_1, R_{ct}) and a constant phase element (CPE_1, CPE_2).

The time constant R_1-CPE$_1$ corresponds to electron transport between the electrocatalyst and the CC electrode, while the second time constant R_{ct}-CPE$_2$ reflects the charge transfer resistance (R_{ct}) at the interface between the electrocatalyst and electrolyte.[20] The R_{ct} values of the bare MoP and the MoP@C samples were calculated to be 4.65 and 2.3 Ω, respectively, thereby confirming a faster Faradaic process for the MoP@C electrocatalyst. In addition, a significantly lower value of R_1 was observed for MoP@C compared to bare MoP (1.33 vs 4.94 Ω), which suggests a lower charge resistance between the MoP@C electrocatalyst and the carbon cloth.

To better understand the influence of the Mo—C and P—C bonds on charge delivery, the electrical transport properties of the electrocatalysts were studied using a Physical Property Measurement System. All measurements were carried out on a pressed pellet, where pores and grain boundaries were responsible for the relatively high resistivities. As indicated in **Figure 5**a, the bare MoP sample exhibited metallic behavior over the whole temperature regime examined, while the MoP@C sample exhibited semiconductor behavior, with a slight decrease in resistivity at higher temperatures. The observed resistivity behavior close to room temperature can be well fitted by the Mott hopping conduction mechanism, neglecting long-range Coulombic interactions between the carriers (Figure 5b). As previously demonstrated, MoP has a complex Fermi surface with valence and conduction bands crossing at different positions in the whole Brillouin zone. Gap opening is therefore difficult due to the topologically protected triple points located below E_F.[8a,9] Therefore, the introduction of a carbon layer is likely responsible for the electron localization in the MoP@C system.[21] Furthermore, Mo—C bonding favors interactions between the Mo-3d and C1-2p orbitals, which localizes the C1-2p orbital and moves its energy level closer to the Fermi level. As a result, the conductivity of MoP@C decreases due to a reduction in the density of the conduction π electrons upon the formation of Mo—C and P—C bonds.[22]

The high intrinsic HER activity of MoP@C prompted us to probe the complicated Volmer step in further detail.[23] In the HER process carried out in alkaline media, the rate of the Volmer step strongly depends on the adsorption free energy of the surface hydrogen and water molecules in addition to the desorption energy of the hydroxide anion. In the case of MoP, a Tafel slope of 102 mV dec^{-1} confirmed that the initial dissociation of water ($M + H_2O + e^- \rightarrow MH^* + OH^-$) is the rate-determining step (Figure 4b). However, in the case of MoP@C, the formation of Mo—C and P—C bonds substantially facilitates the HER kinetics. More specifically, the density of states close to the Fermi level is enlarged due to the accumulation of localized electrons, thereby leading to the down shifting of the valence and conduction bands of MoP@C. Discharge of the localized electrons thus becomes more facile and electron mobility is enhanced (Figure 4d) due to the sufficiently high Fermi energy.[13d,23,24] In addition, Mo—C bonding optimizes the free energy barriers that favor the adsorption and desorption of hydrogen.[13d,25] This promotes the dissociation of water to H* intermediates and leads to rapid HER kinetics (Figure 5c). Furthermore, as confirmed by XPS, the binding energy of the P 2p component in the P—C bond (133.0 eV) is significantly larger than that in P^0 (130.2 eV)[4b] and MoP (129.3 eV) (Figure 3b),

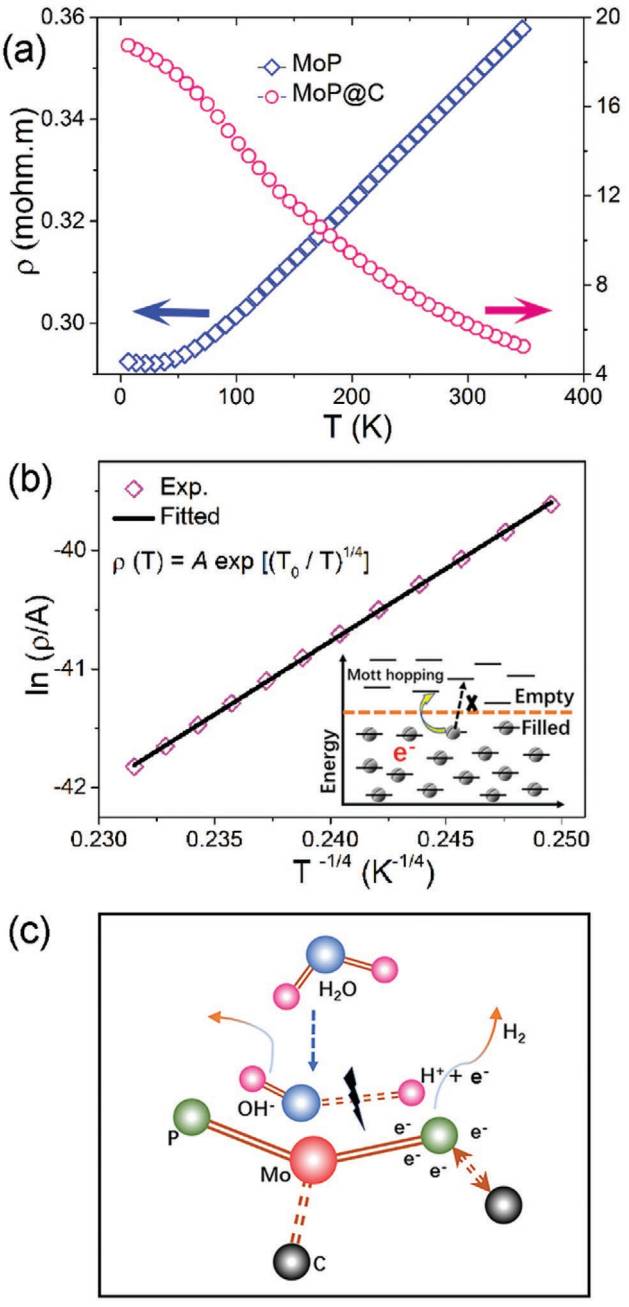

Figure 5. a) Electrical transport and b) Mott hopping conductivity models. c) Illustration of the C—Mo and P—Mo bonding that favors water dissociation and hydrogen reduction in an alkaline medium.

implying charge transfer from P to C through P—C bonding. The electron density withdrawn from P is then donated back to the vacant d orbitals of Mo, thereby accelerating the sluggish Volmer process with a much smaller Tafel slope (Figure 4b).[26]

In summary, we have designed and developed a novel HER electrocatalyst based on MoP embedded in Mo- and P-codoped carbon. Due to the formation of abundant Mo—C and P—C bonds at the interface between the MoP particles and the carbon layer, the Fermi level of the MoP@C electrocatalyst favors the transport of electrons. As a result, MoP@C

exhibits particularly high HER activity compared to that of Pt/C when an alkaline solution is employed as the electrolyte. Furthermore, the accumulation of electrons and the discharge of localized electrons results in an ultrahigh exchange current density. We therefore conclude that this work sheds new light on the correlation between the topological properties and electrocatalytic performances of MoP and related materials, potentially leading to novel engineered materials in their topological states for use as highly active and efficient electrocatalysts in hydrogen evolution, oxygen evolution, and CO_2 reduction processes.

Supporting Information

Supporting Information is available from the Wiley Online Library or from the author.

Acknowledgements

The authors gratefully acknowledge Steffen Hückmann and Yurii Prots for the PXRD measurements, Marcus Schmidt for TG/DTA analysis, and Ralf Koban for transport measurements. The authors would also like to thank Dr. Wujun Shi and Dr. Qiunan Xu for their helpful discussions. In addition, the authors thank ZOLTEK for providing the carbon cloth employed herein. This work was financially supported by the European Research Council (ERC Advanced Grant No. 291472 "Idea Heusler") and ERC Advanced Grant (No. 742068). J.Z. and X.F. thank the support of the ERC Grant on 2DMATER, EC under Graphene Flagship (No. CNECT-ICT-604391), and cfaed (Center for Advancing Electronics Dresden).

Conflict of Interest

The authors declare no conflict of interest.

Keywords

electrocatalysts, hydrogen evolution reaction, MoP, topological semimetals

Received: April 26, 2018
Revised: May 24, 2018
Published online: June 25, 2018

[1] J. Zhang, T. Wang, P. Liu, S. Liu, R. Dong, X. Zhuang, M. Chen, X. Feng, *Energy Environ. Sci.* **2016**, *9*, 2789.
[2] a) X. Zou, Y. Zhang, *Chem. Soc. Rev.* **2015**, *44*, 5148; b) G. Li, G. R. Blake, T. T. Palstra, *Chem. Soc. Rev.* **2017**, *46*, 1693.
[3] a) V. R. Stamenkovic, D. Strmcnik, P. P. Lopes, N. M. Markovic, *Nat. Mater.* **2016**, *16*, 57; b) X. D. Wang, Y. Cao, Y. Teng, H. Y. Chen, Y. F. Xu, D. B. Kuang, *ACS Appl. Mater. Interfaces* **2017**, *9*, 32812; c) C. Zhang, Y. Huang, Y. Yu, J. Zhang, S. Zhuo, B. Zhang, *Chem. Sci.* **2017**, *8*, 2769.
[4] a) J. Kibsgaard, T. F. Jaramillo, *Angew. Chem.* **2014**, *53*, 14433; b) Z. Xing, Q. Liu, A. M. Asiri, X. Sun, *Adv. Mater.* **2014**, *26*, 5702; c) A. Wu, C. Tian, H. Yan, Y. Jiao, Q. Yan, G. Yang, H. Fu, *Nanoscale* **2016**, *8*, 11052; d) Y.-Y. Ma, C.-X. Wu, X.-J. Feng, H.-Q. Tan, L.-K. Yan, Y. Liu, Z.-H. Kang, E.-B. Wang, Y.-G. Li, *Energy Environ. Sci.* **2017**, *10*, 788; e) X.-D. Wang, Y.-F. Xu, H.-S. Rao, W.-J. Xu, H.-Y. Chen, W.-X. Zhang, D.-B. Kuang, C.-Y. Su, *Energy Environ. Sci* **2016**, *9*, 1468; f) X.-D. Wang, H.-Y. Chen, Y.-F. Xu, J.-F. Liao, B.-X. Chen, H.-S. Rao, D.-B. Kuang, C.-Y. Su, *J. Mater. Chem. A* **2017**, *5*, 7191.
[5] P. Xiao, M. A. Sk, L. Thia, X. Ge, R. J. Lim, J.-Y. Wang, K. H. Lim, X. Wang, *Energy Environ. Sci.* **2014**, *7*, 2624.
[6] a) B. Yan, C. Felser, *Annu. Rev. Condens. Matter Phys.* **2016**, *8*, 1; b) A. A. Burkov, *Nat. Mater.* **2016**, *15*, 1145.
[7] C. Shekhar, A. K. Nayak, Y. Sun, M. Schmidt, M. Nicklas, I. Leermakers, U. Zeitler, Y. Skourski, J. Wosnitza, Z. Liu, Y. Chen, W. Schnelle, H. Borrmann, Y. Grin, C. Felser, B. Yan, *Nat. Phys.* **2015**, *11*, 645.
[8] a) B. Q. Lv, Z. L. Feng, Q. N. Xu, X. Gao, J. Z. Ma, L. Y. Kong, P. Richard, Y. B. Huang, V. N. Strocov, C. Fang, H. M. Weng, Y. G. Shi, T. Qian, H. Ding, *Nature* **2017**, *546*, 627; b) Z. Chi, X. Chen, C. An, L. Yang, J. Zhao, Z. Feng, Y. Zhou, Y. Zhou, C. Gu, B. Zhang, Y. Yuan, C. Kenney-Benson, W. Yang, G. Wu, X. Wan, Y. Shi, X. Yang, Z. Yang, *npj Quantum Materials* **2018**, *3*, https://doi.org/10.1038/s41535-018-0102-7.
[9] C. Shekhar, Y. Sun, N. Kumar, M. Nicklas, K. Manna, V. Suess, O. Young, I. Leermakers, T. Foerster, M. Schmidt, L. Muechler, P. Werner, W. Schnelle, U. Zeitler, B. Yan, S. S. P. Parkin, C. Felser, **2017**, arXiv:1703.03736 [cond-mat.mtrl-sci].
[10] Q. Wu, S. Zhang, H. Song, M. Troyer, A. A. Soluyanov. *Comput. Phys. Commun.* **2018**, *224*, 405.
[11] a) C. Du, H. Huang, Y. Wu, S. Wu, W. Song, *Nanoscale* **2016**, *8*, 16251; b) J. Yang, F. Zhang, X. Wang, D. He, G. Wu, Q. Yang, X. Hong, Y. Wu, Y. Li, *Angew. Chem.* **2016**, *55*, 12854.
[12] a) K. Ojha, M. Sharma, H. Kolev, A. K. Ganguli, *Catal. Sci. Technol.* **2017**, *7*, 668; b) W. Cui, Q. Liu, Z. Xing, A. M. Asiri, K. A. Alamry, X. Sun, *Appl. Catal., B* **2015**, *164*, 144.
[13] a) W. Cui, N. Cheng, Q. Liu, C. Ge, A. M. Asiri, X. Sun, *ACS Catal.* **2014**, *4*, 2658; b) Z.-Y. Wu, B.-C. Hu, P. Wu, H.-W. Liang, Z.-L. Yu, Y. Lin, Y.-R. Zheng, Z. Li, S.-H. Yu, *NPG Asia Mater.* **2016**, *8*, e288; c) C. R. Ryder, J. D. Wood, S. A. Wells, Y. Yang, D. Jariwala, T. J. Marks, G. C. Schatz, M. C. Hersam, *Nat. Chem.* **2016**, *8*, 597; d) J. S. Li, Y. Wang, C. H. Liu, S. L. Li, Y. G. Wang, L. Z. Dong, Z. H. Dai, Y. F. Li, Y. Q. Lan, *Nat. Commun.* **2016**, *7*, 11204; e) L. Lin, W. Zhou, R. Gao, S. Yao, X. Zhang, W. Xu, S. Zheng, Z. Jiang, Q. Yu, Y. W. Li, C. Shi, X. D. Wen, D. Ma, *Nature* **2017**, *544*, 80.
[14] J. Sun, G. Zheng, H. W. Lee, N. Liu, H. Wang, H. Yao, W. Yang, Y. Cui, *Nano Lett.* **2014**, *14*, 4573.
[15] L. Daasch, D. Smith, *Anal. Chem.* **1951**, *23*, 853.
[16] H. B. Wu, B. Y. Xia, L. Yu, X. Y. Yu, X. W. Lou, *Nat. Commun.* **2015**, *6*, 6512.
[17] J. Tian, Q. Liu, A. M. Asiri, X. Sun, *J. Am. Chem. Soc.* **2014**, *136*, 7587.
[18] Y. Liang, Q. Liu, A. M. Asiri, X. Sun, Y. Luo, *ACS Catal.* **2014**, *4*, 4065.
[19] Y. Zheng, Y. Jiao, M. Jaroniec, S. Z. Qiao, *Angew. Chem.* **2015**, *54*, 52.
[20] X. Wang, Y. V. Kolen'ko, X. Q. Bao, K. Kovnir, L. Liu, *Angew. Chem.* **2015**, *54*, 8188.
[21] a) G. Li, B. Zhang, J. Rao, D. Herranz Gonzalez, G. R. Blake, R. A. de Groot, T. T. M. Palstra, *Chem. Mater.* **2015**, *27*, 8220; b) F. Alibart, M. Lejeune, O. Durand Drouhin, K. Zellama, M. Benlahsen, *J. Appl. Phys.* **2010**, *108*, 053504.
[22] P. N. Vishwakarma, S. V. Subramanyam, *J. Appl. Phys.* **2006**, *100*, 113702.
[23] Z. Pu, I. S. Amiinu, Z. Kou, W. Li, S. Mu, *Angew. Chem.* **2017**, *129*, 11717 .
[24] a) R. He, J. Hua, A. Zhang, C. Wang, J. Peng, W. Chen, J. Zeng, *Nano Lett.* **2017**, *17*, 4311; b) S. Guo, Z. Deng, M. Li, B. Jiang, C. Tian, Q. Pan, H. Fu, *Angew. Chem., Int. Ed.* **2016**, *55*, 1830.
[25] C. Lu, D. Tranca, J. Zhang, F. N. Rodri Guez Hernandez, Y. Su, X. Zhuang, F. Zhang, G. Seifert, X. Feng, *ACS Nano* **2017**, *11*, 3933.
[26] a) M. A. R. Anjum, J. S. Lee, *ACS Catal.* **2017**, *7*, 3030; b) Y. Liu, G. G. Yu, D. Li, Y. Sun, T. Asefa, W. Chen, X. Zou, *Angew. Chem.* **2015**, *54*, 10752.